

Imprint of SUSY in radiative B meson decays

K. Hidaka
Tokyo Gakugei University

Collaboration with
H. Eberl, E. Ginina (HEPHY, Vienna),
A. Ishikawa (BELLE II, KEK, Tsukuba)

Reference: arXiv:2106.15228 [hep-ph]

SUSY2021, 23 Aug 2021, 'Beijing'

Contents

1. Introduction

2. MSSM with QFV

3. Constraints on the MSSM

4. Parameter scan in the MSSM

5. WCs C_7 and C'_7 in the MSSM with QFV

6. Conclusion

1. Introduction

- We study **supersymmetric (SUSY) effects on $C_7(\mu_b)$ and $C'_7(\mu_b)$** which are the Wilson coefficients (WCs) for $b \rightarrow s$ gamma at b -quark mass scale μ_b and are closely related to **radiative B meson decays**.
- The SUSY-loop contributions to the **$C_7(\mu_b)$ and $C'_7(\mu_b)$** are calculated in the Minimal Supersymmetric Standard Model (MSSM) with **general quark flavor violation (QFV)**.
- In the computation of the WCs, **for the first time** we perform a systematic **MSSM parameter scan** respecting all the relevant theoretical and experimental constraints, such as those from K - & B -meson and $H(125)$ data and recent limits on Supersymmetric (SUSY) particle masses from LHC experiments.
- Here we study a possibility that **imprint of SUSY** can be found in radiative B meson decays, focusing on the WCs **$C_7(\mu_b)$ and $C'_7(\mu_b)$** .

2. MSSM with QFV

Key parameters in this study are:

** QFV parameters: $\tilde{c}_{L/R} - \tilde{t}_{L/R}$ & $\tilde{s}_{L/R} - \tilde{b}_{L/R}$ mixing parameters*

** QFC parameter: $\tilde{t}_L - \tilde{t}_R$ & $\tilde{b}_L - \tilde{b}_R$ mixing parameters*

$M^2_{Q23} = (\tilde{c}_L - \tilde{t}_L$ mixing parameter)

$M^2_{U23} = (\tilde{c}_R - \tilde{t}_R$ mixing parameter)

$M^2_{D23} = (\tilde{s}_R - \tilde{b}_R$ mixing parameter)

$T_{U23} = (\tilde{c}_R - \tilde{t}_L$ mixing parameter)

$T_{U32} = (\tilde{c}_L - \tilde{t}_R$ mixing parameter)

$T_{U33} = (\tilde{t}_L - \tilde{t}_R$ mixing parameter)

$T_{D23} = (\tilde{s}_R - \tilde{b}_L$ mixing parameter)

$T_{D32} = (\tilde{s}_L - \tilde{b}_R$ mixing parameter)

$T_{D33} = (\tilde{b}_L - \tilde{b}_R$ mixing parameter)

3. Constraints on the MSSM

We respect the following experimental and theoretical constraints:

- (1) The recent LHC limits on the masses of squarks, sleptons, gluino, charginos and neutralinos.*
- (2) The constraint on $(m_{A/H^+}, \tan\beta)$ from recent MSSM Higgs boson search at LHC.*
- (3) The constraints on the QFV parameters from the B & K meson data.*

$$B(b \rightarrow s \gamma) \quad \Delta M_{B_s} \quad B(B_s \rightarrow \mu^+ \mu^-) \quad B(B_u^+ \rightarrow \tau^+ \nu) \quad \textit{etc.}$$

- (4) The constraints from the observed Higgs boson mass and couplings at LHC ; e.g.
 $121.6 \text{ GeV} < m_{h^0} < 128.6 \text{ GeV}$ (allowing for theoretical uncertainty) ,
 $0.71 < \kappa_b < 1.43$ (ATLAS), $0.56 < \kappa_b < 1.70$ (CMS)*
- (5) The experimental limit on SUSY contributions to the electroweak ρ parameter
 $\Delta\rho(\text{SUSY}) < 0.0012$.*
- (6) Theoretical constraints from the vacuum stability conditions for the trilinear couplings $T_{U\alpha\beta}$ and $T_{D\alpha\beta}$.*

4. Parameter scan in the MSSM

- We compute the WCs $C_7(\mu_b)$ and $C'_7(\mu_b)$ at LO in the **MSSM** with **QFV**.
- We take parameter scan ranges as follows:

$$1 \text{ TeV} < M_{\text{SUSY}} < 5 \text{ TeV}$$

$$10 < \tan\beta < 80$$

$$2500 < M_3 < 5000 \text{ GeV}$$

$$100 < M_2 < 2500 \text{ GeV}$$

$$100 < M_1 < 2500 \text{ GeV}$$

$$100 < \mu < 2500 \text{ GeV}$$

$$1350 < m_A(\text{pole}) < 6000 \text{ GeV}$$

etc. etc.

- **In the parameter scan, all of the relevant experimental and theoretical constraints are imposed.**
- **8660000** parameter points are generated and **72904** points survive the constraints.

5. WC's $C_7(\mu_b)$ and $C'_7(\mu_b)$ in the MSSM with QFV

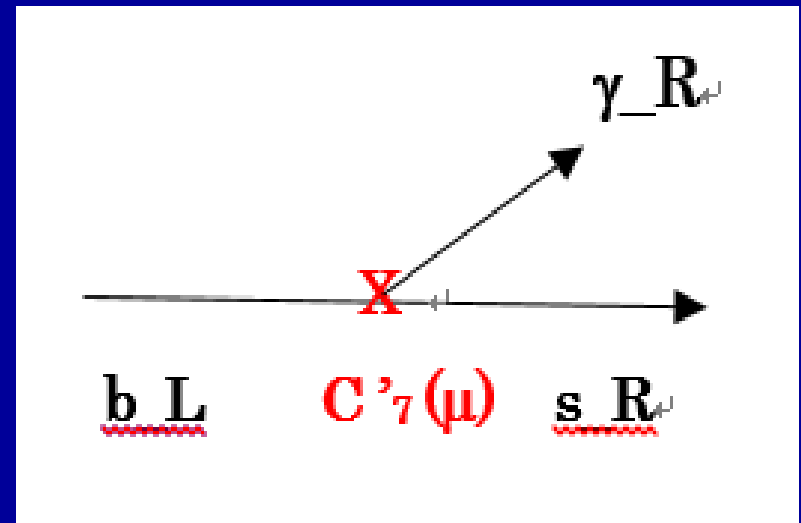
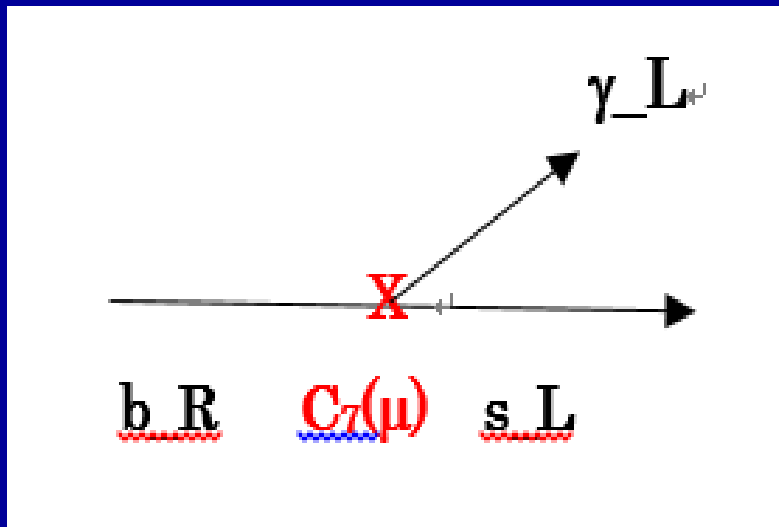
Low-energy effective Hamiltonian, at the bottom mass scale μ_b :

$$\mathcal{H}_{eff} = -\frac{4G_F}{\sqrt{2}} V_{tb} V_{ts}^* \sum_i C_i(\mu_b) Q_i(\mu_b) .$$

$$\begin{aligned} Q_2 &= \bar{s}_L \gamma_\mu c_L \bar{c}_L \gamma^\mu b_L , \\ C_7 \quad Q_7 &= \frac{e}{16\pi^2} m_b \bar{s}_L \sigma^{\mu\nu} b_R F_{\mu\nu} , \\ C_8 \quad Q_8 &= \frac{g_s}{16\pi^2} m_b \bar{s}_L \sigma^{\mu\nu} G_{\mu\nu}^a T_a b_R . \\ Q'_2 &= \bar{s}_R \gamma_\mu c_R \bar{c}_R \gamma^\mu b_R , \\ C'_7 \quad Q'_7 &= \frac{e}{16\pi^2} m_b \bar{s}_R \sigma^{\mu\nu} b_L F_{\mu\nu} , \\ C'_8 \quad Q'_8 &= \frac{e}{16\pi^2} m_b \bar{s}_R \sigma^{\mu\nu} G_{\mu\nu}^a T_a b_L . \end{aligned}$$

(Note) $C'_{7,8}(\mu) \approx 0$ in SM

- We compute the WCs $C_7(\mu_b)$ and $C'_7(\mu_b)$ at b -quark mass scale μ_b at LO in the *MSSM with QFV*.



- The WCs $C_7(\mu_b)$ and $C'_7(\mu_b)$ can be measured precisely at *BELLE II & LHCb-Upgrade!*

We compute $C_{7,8}(\mu_W)$ and $C'_{7,8}(\mu_W)$ at weak scale μ_W at LO in the MSSM with QFV.



Then we compute $C_7(\mu_b)$ and $C'_7(\mu_b)$ at b -quark mass scale μ_b by using RG QCD scale evolution at LL.

RG QCD scale evolution at LO:

$$C_7(\mu_W) / C'_7(\mu_W) \rightarrow C_7(\mu_b) / C'_7(\mu_b)$$

$(\mu_W = 160 \text{ GeV} \text{ and } \mu_b = 4.8 \text{ GeV})$

- $C_7(\mu_b) = \eta^{(16/23)} C_7(\mu_W) + (8/3)(\eta^{(14/23)} - \eta^{(16/23)}) C_8(\mu_W) + (\sum_{i=1-8} h_i \eta^{a_i})$
- $C'_7(\mu_b) = \eta^{(16/23)} C'_7(\mu_W) + (8/3)(\eta^{(14/23)} - \eta^{(16/23)}) C'_8(\mu_W)$

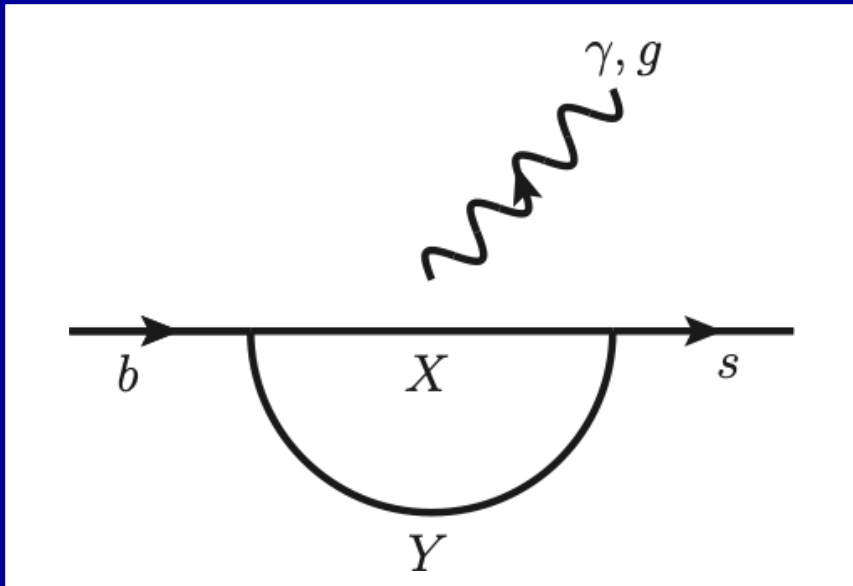
With

$$\eta = \alpha_s(\mu_W) / \alpha_s(\mu_b)$$

$$h_i = (626126/272277, -56281/51730, -3/7, -1/14, -0.6494, -0.0380, -0.0186, -0.0057)$$

$$a_i = (14/23, 16/23, 6/23, -12/23, 0.4086, -0.4230, -0.8994, 0.1456)$$

1-Loop contributions to $C_{7,8}(\mu_W)$ and $C'_{7,8}(\mu_W)$ at weak scale $\mu_W = 160 \text{ GeV}$



SM one-loop contributions:

$$(X, Y) = (t/c/u, W^+)$$

MSSM one-loop contributions:

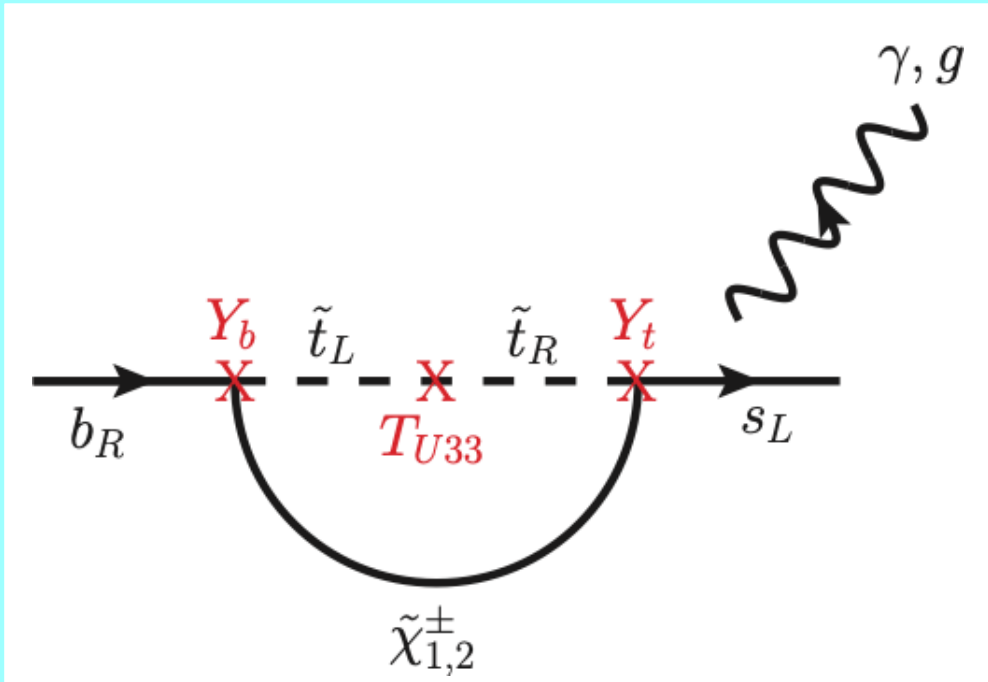
$$(X, Y) = (\text{stop/scharm, chargino}),$$
$$(\text{sbottom/ssstrange, gluino}),$$
$$(\text{sbottom/ssstrange, neutralino}),$$
$$(t/c/u, H^+)$$

$\tilde{t}_L - \tilde{t}_R$ loop contributions to $C_{7,8}(\mu_W)$:

$$\tilde{\chi}^\pm \sim \tilde{W}^\pm + \tilde{H}^\pm$$

Y_b : bottom Yukawa

Y_t : top Yukawa

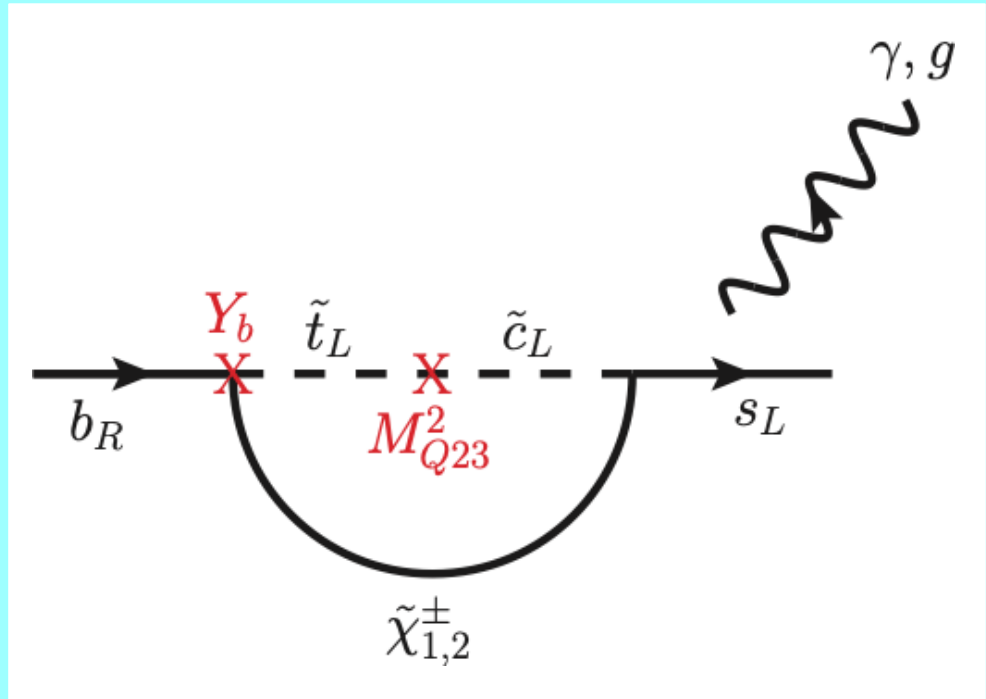


$\tilde{t}_L - \tilde{t}_R$ loop contributions to $C_{7,8}(\mu_W)$ can be enhanced by large trilinear couplings T_{U33} and large Y_b for large $\tan\beta$ and large Y_t !

$\tilde{t} - \tilde{c}$ loop contributions to $C_{7,8}(\mu_W)$:

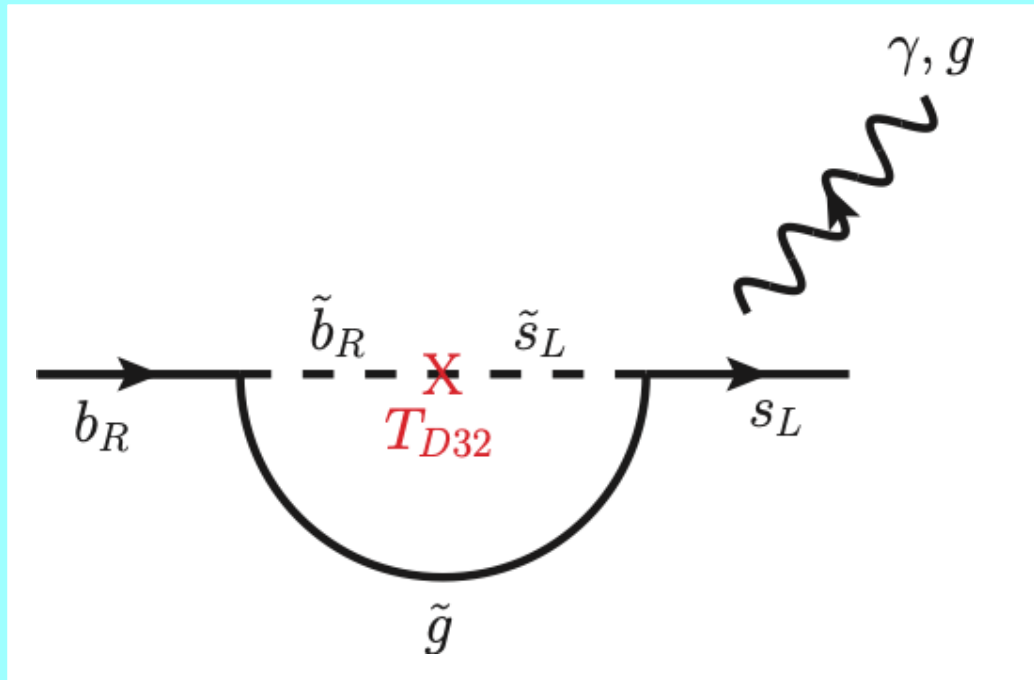
$$\tilde{\chi}^\pm \sim \tilde{W}^\pm + \tilde{H}^\pm$$

Y_b : bottom Yukawa



$\tilde{t} - \tilde{c}$ loop contributions to $C_{7,8}(\mu_W)$ can be enhanced by large $\tilde{t}_L - \tilde{c}_L$ mixing term M_{Q23}^2 and large Y_b for large $\tan\beta$!

$\tilde{b} - \tilde{s}$ loop contributions to $C_{7,8}(\mu_W)$:

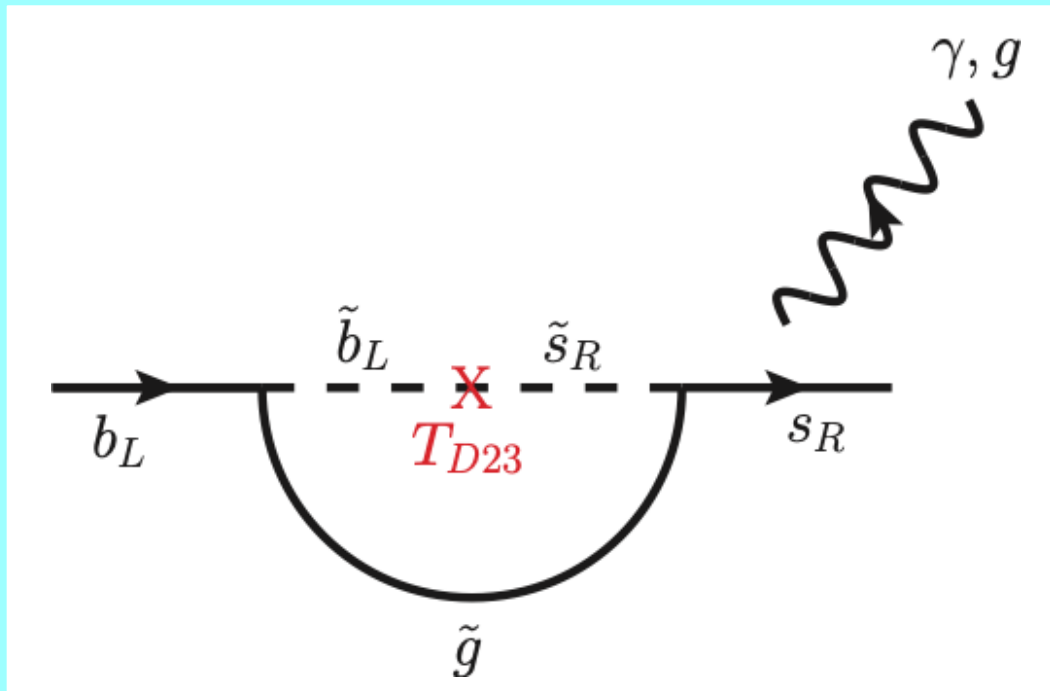


$|T_{D32}|$ is controlled by Y_b due to vacuum stability condition.



$\tilde{b} - \tilde{s}$ loop contributions to $C_{7,8}(\mu_W)$ can be enhanced by large trilinear coupling T_{D32} and large Y_b for large $\tan\beta$!

$\tilde{b} - \tilde{s}$ loop contributions to $C'_{7,8}(\mu_W)$:



$|T_{D23}|$ is controlled by Y_b due to vacuum stability condition.



$\tilde{b} - \tilde{s}$ loop contributions to $C'_{7,8}(\mu_W)$ can be enhanced by large trilinear coupling T_{D23} and large Y_b for large $\tan\beta$!

Considering higher order MI contributions to the WCs $C_{7,8}$ & $C'_{7,8}$, MIs of $T_{U23,32}$, T_{D33} , M^2_{U23} and M^2_{D23} can also contribute to the WCs!



- large trilinear couplings $T_{U23,32,33}$ & $T_{D23,32,33}$*
- large QFV soft-mass-terms M^2_{Q23} , M^2_{U23} , M^2_{D23}*
- large Y_b for large $\tan\beta$ and large Y_t*

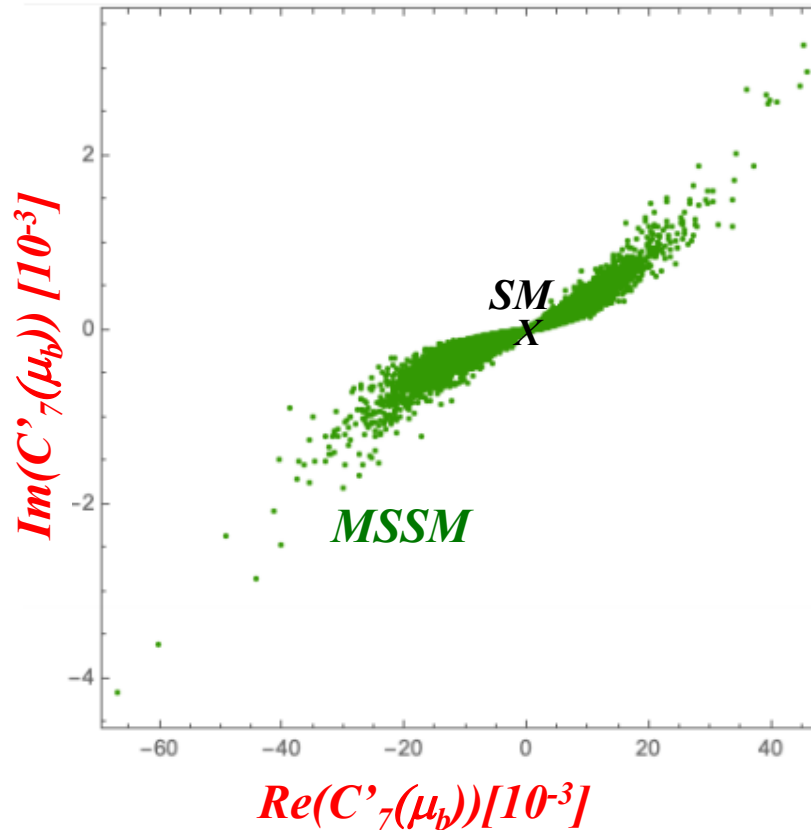


Large MSSM one-loop contributions to $C_{7,8}(\mu_W)$ and $C'_{7,8}(\mu_W)$ at weak scale μ_W !



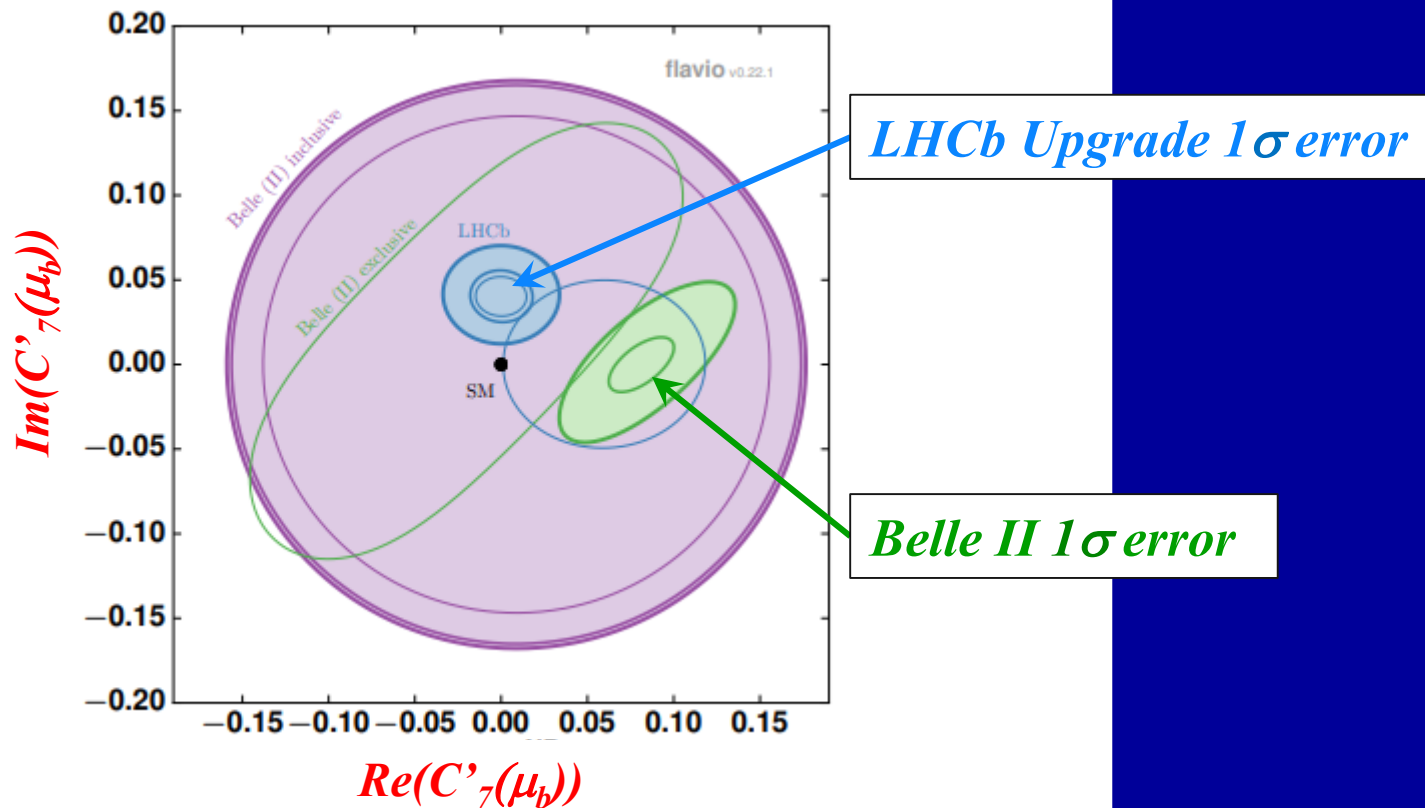
Large MSSM one-loop contributions to $C_7(\mu_b)$ and $C'_7(\mu_b)$ at b -quark mass scale μ_b !

Scatter Plot in $ReC'_7(\mu_b)$ - $ImC'_7(\mu_b)$ plane



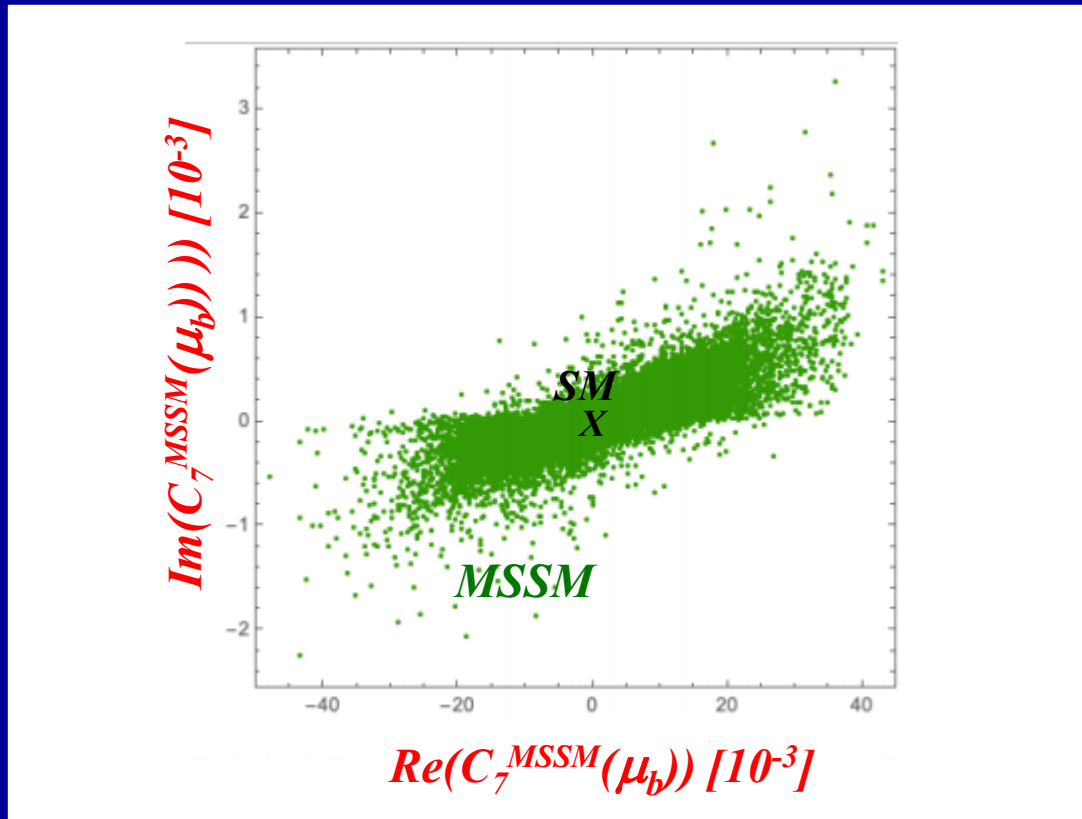
The MSSM contribution to $Re(C'_7(\mu_b))$ can be as large as ~ -0.07 which could correspond to about 4σ New Physics (NP) signal significance in future LHCb Upgrade and Belle II experiments.

Expected 1σ errors of $ReC'_7(\mu_b)-ImC'_7(\mu_b)$ obtained from future LHCb Upgrade and Belle II



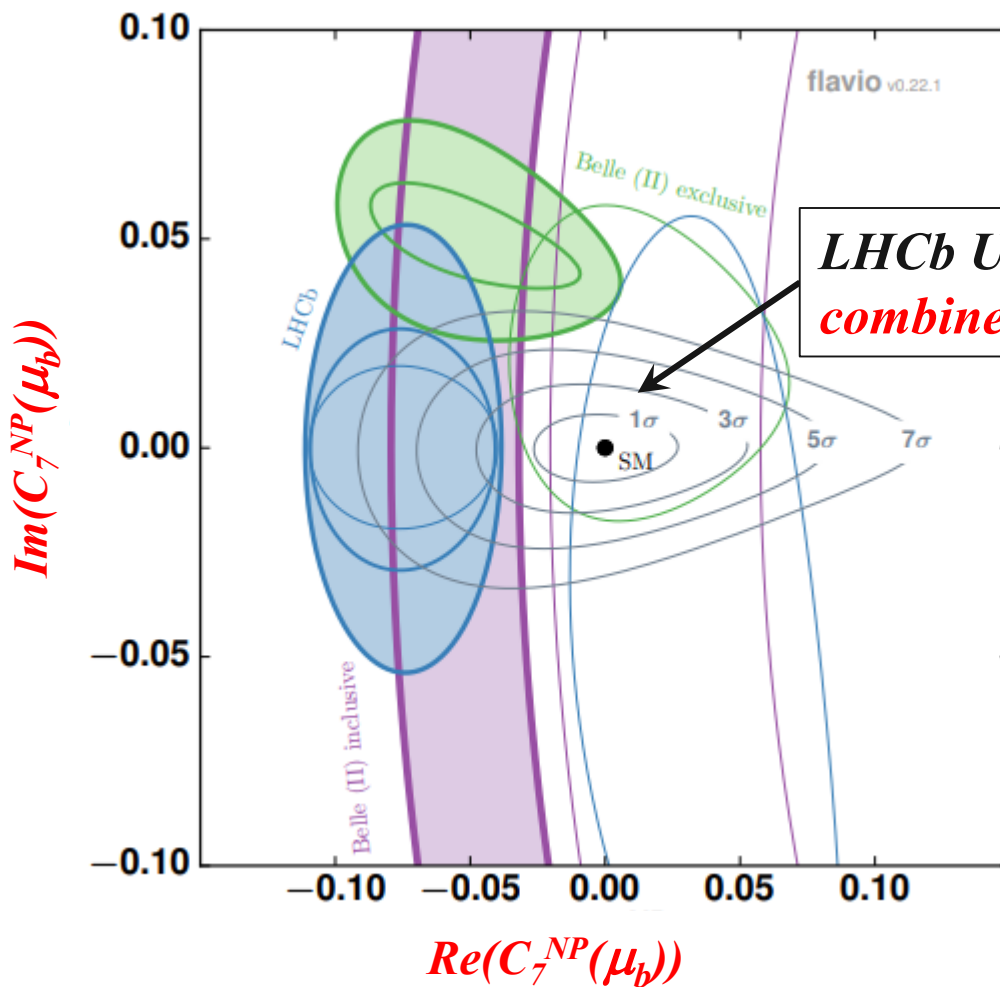
*Belle II Physics Book, arXiv:1808.10567;
LHCb II Physics Book, arXiv:1808.08865;
Albrecht et al., arXiv:1709.10308.*

Scatter Plot in $ReC_7^{MSSM}(\mu_b)$ - $ImC_7^{MSSM}(\mu_b)$ plane



The MSSM contribution to $Re(C_7(\mu_b))$ can be as large as ~ -0.05 which could correspond to about 3σ NP signal significance in future LHCb and Belle II experiments.

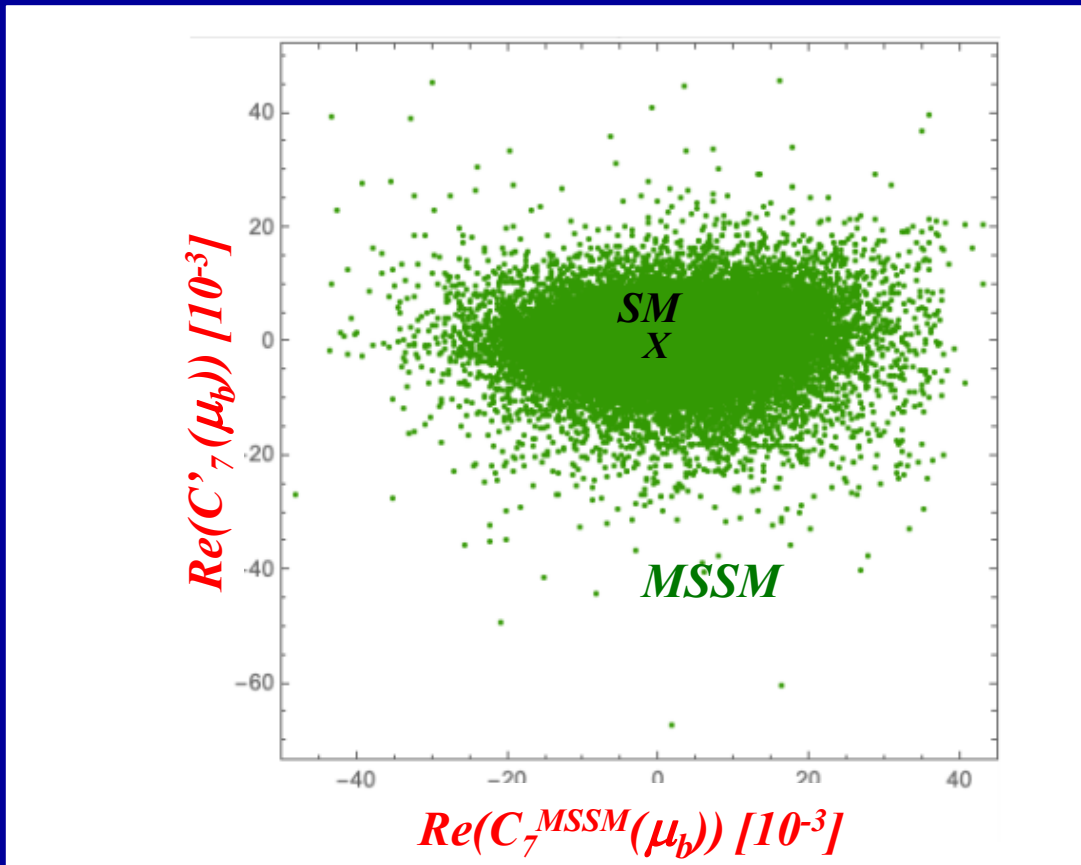
Expected errors of $ReC_7^{NP}(\mu_b)$ - $ImC_7^{NP}(\mu_b)$ obtained from future LHCb Upgrade and Belle II



**LHCb Upgrade and Belle II
combined 3σ error**

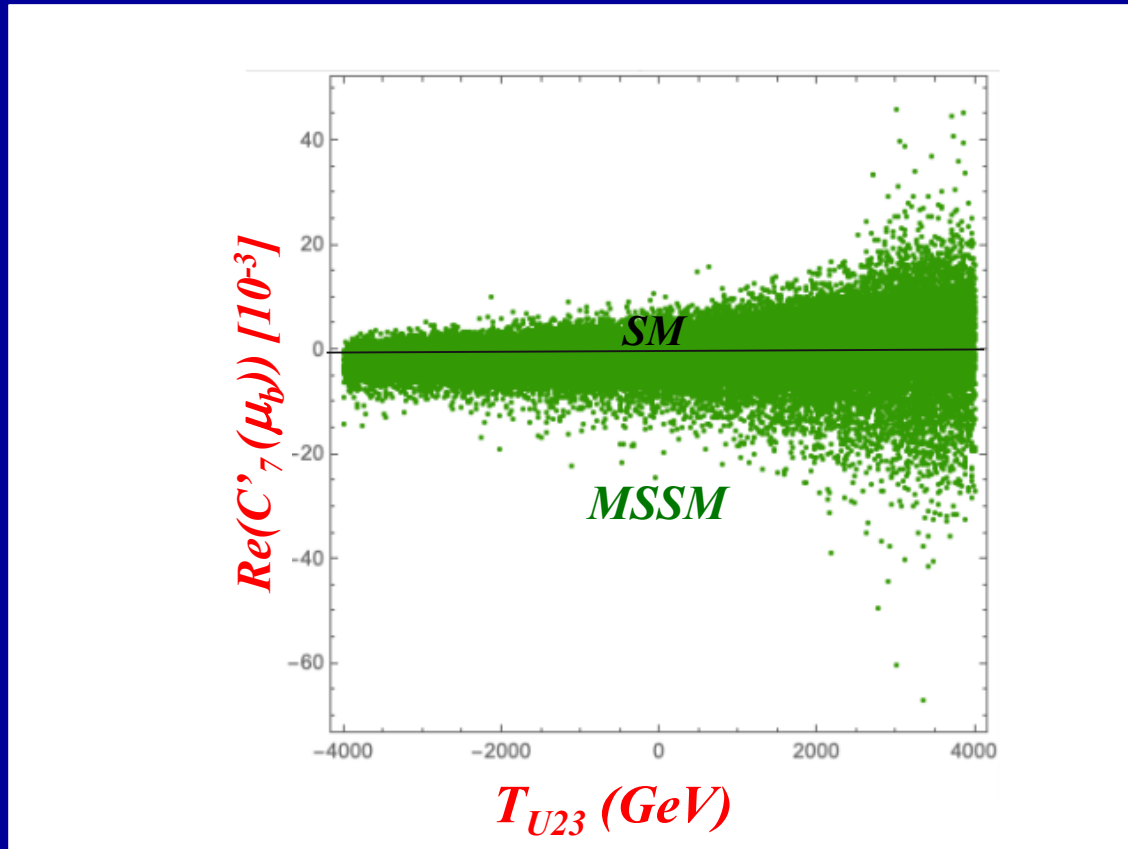
*Belle II Physics Book, arXiv:1808.10567;
LHCb II Physics Book, arXiv:1808.08865;
Albrecht et al., arXiv:1709.10308.*

Scatter Plot in $ReC_7^{MSSM}(\mu_b)$ - $ReC'_7(\mu_b)$ plane



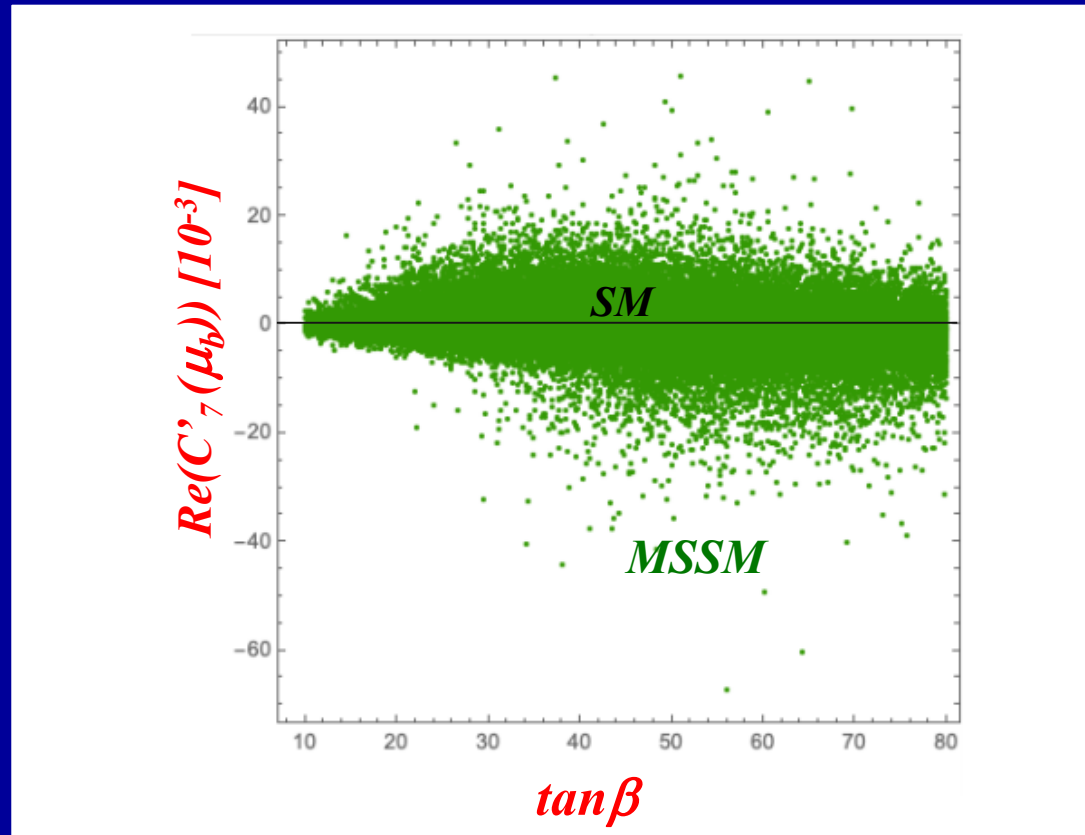
$Re(C_7^{MSSM}(\mu_b))$ and $Re(C'_7(\mu_b))$ can be quite sizable simultaneously!

Scatter plot in $T_{U23} - \text{Re}(C'_7(\mu_b))$ plane



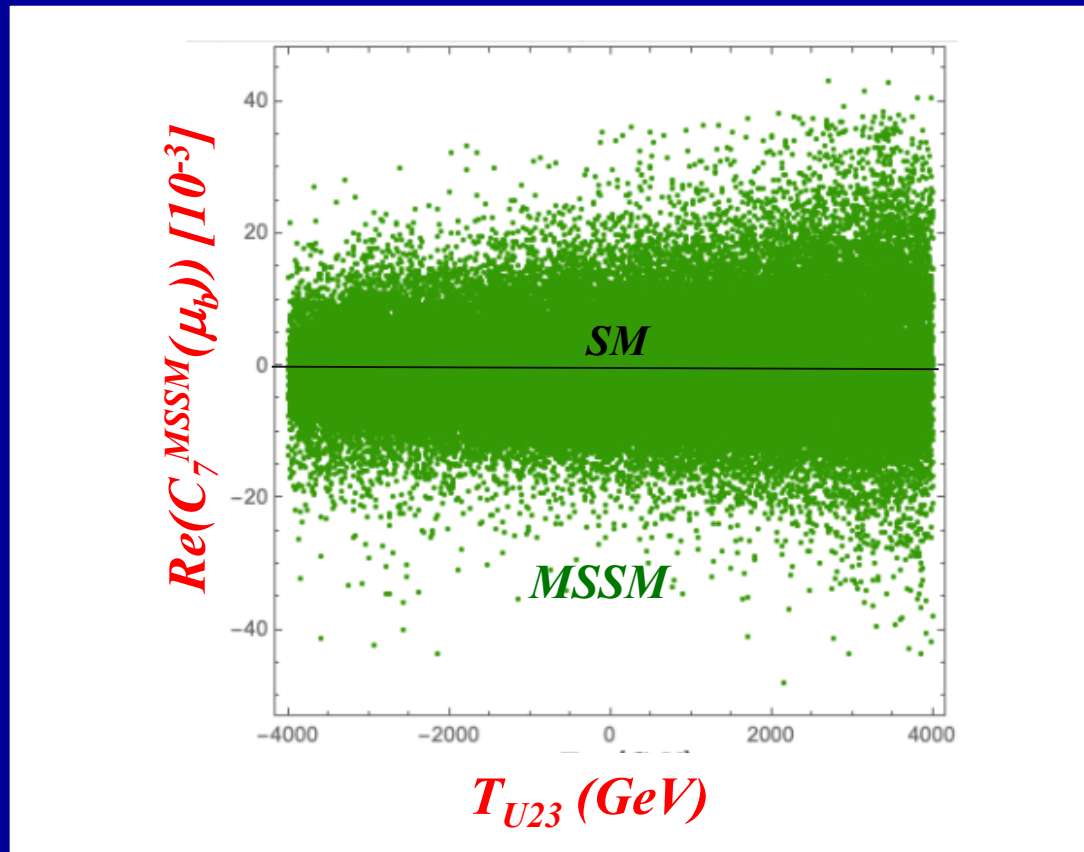
- *MSSM one-loop contributions to $\text{Re}(C'_7(\mu_b))$ can be large (-0.07 ~ +0.05) for large T_{U23} (> 0)!*
- *$\text{Re}(C'_7(\mu_b)) \approx 0$ (SM)*

Scatter plot in $\tan\beta - \text{Re}(C'_7(\mu_b))$ plane



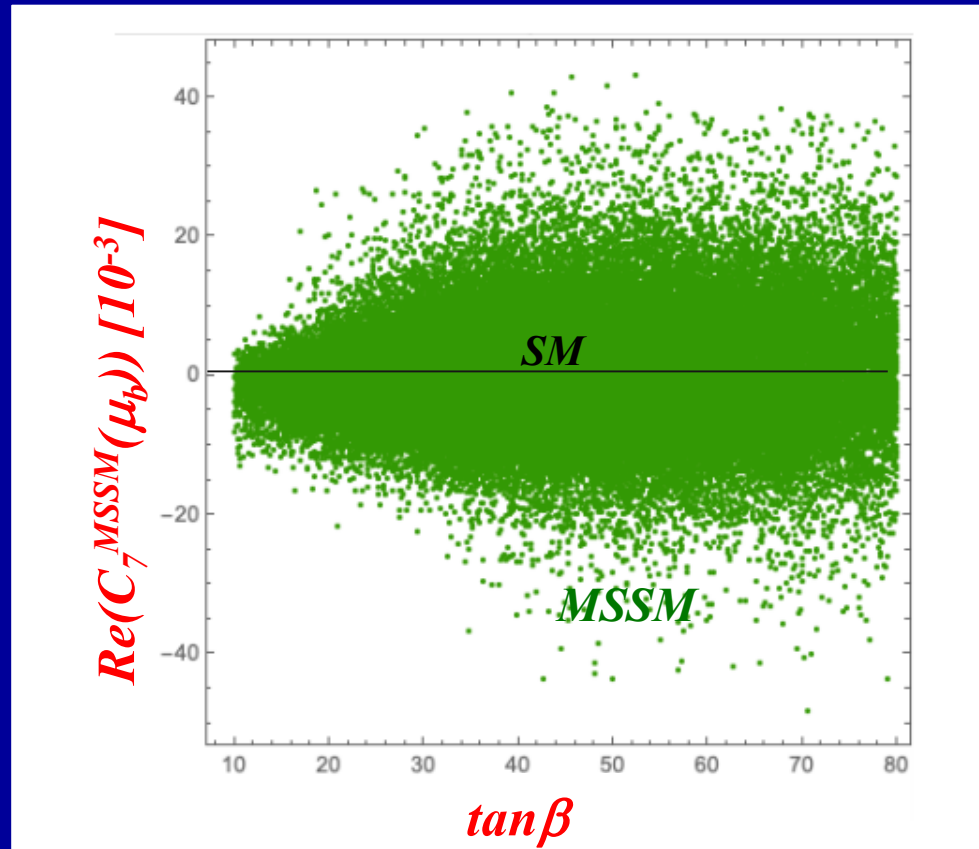
- *MSSM one-loop contributions to $\text{Re}(C'_7(\mu_b))$ can be large ($-0.07 \sim +0.05$) for large $\tan\beta (> 40)$!*
- *This behavior is consistent with our expectation!*

Scatter plot in $T_{U23} - \text{Re}(C_7^{MSSM}(\mu_b))$ plane



- *MSSM one-loop contributions to $\text{Re}(C_7(\mu_b))$ can be large ($\sim \pm 0.05$) for large $T_{U23} (> 0)$!*

Scatter plot in $\tan\beta - \text{Re}(C_7^{\text{MSSM}}(\mu_b))$ plane



- *MSSM one-loop contributions to $\text{Re}(C_7(\mu_b))$ can be large ($\sim \pm 0.05$) for large $\tan\beta (> 40)$!*
- *This behavior is consistent with our expectation!*

6. Conclusion

- *We have studied **SUSY effects on $C_7(\mu_b)$ and $C'_7(\mu_b)$** which are the Wilson coefficients for $b \rightarrow s$ gamma at b-quark mass scale μ_b and are closely related to radiative B meson decays.*
- *The **SUSY-loop contributions to the $C_7(\mu_b)$ and $C'_7(\mu_b)$** are calculated in the **MSSM with general quark flavor violation (QFV)** and real parameters at LO.*
- *In the computation of the WCs, **for the first time**, we have performed a **systematic MSSM parameter scan** respecting all the relevant constraints, i.e. theoretical constraints from vacuum stability conditions and experimental constraints, such as those from K- & B-meson data and electroweak precision data, as well as recent limits on SUSY particle masses and H(125) data from LHC experiments.*

- *From the parameter scan, we have found the following:*

(1) The MSSM contribution to $Re(C_7(\mu_b))$ can be as large as $\sim \pm 0.05$ which could correspond to about 3σ New Physics (NP) signal significance in future LHCb Upgrade and Belle II experiments.

(2) The MSSM contribution to $Re(C'_7(\mu_b))$ can be as large as ~ -0.08 which could correspond to about 4σ NP signal significance in future LHCb Upgrade and Belle II experiments.

(3) These large MSSM contributions to the WC's are mainly due to
- large $\tilde{c} - \tilde{t}$ mixing & large \tilde{c} / \tilde{t} trilinear couplings $T_{U23}, T_{U32}, T_{U33}$,
- large $\tilde{s} - \tilde{b}$ mixing & large \tilde{s} / \tilde{b} trilinear couplings $T_{D23}, T_{D32}, T_{D33}$,
- large Y_b for large $\tan\beta$ and large Y_t .

- *In case such large New Physics contributions to the WCs are really observed in the future experiments at Belle II and LHCb Upgrade, it could be the imprint of QFV SUSY (MSSM with QFV) and would encourage to perform further studies of the WCs at NLO/NNLO level in this model.*

- *Our analysis suggests the following:*

PETRA/TRISTAN $e^- e^+$ collider discovered virtual Z^0 effect for the first time.

Later, CERN $p \bar{p}$ collider discovered the Z^0 boson.

Similarly, Belle II / LHCb Upgrade could discover virtual Sparticle effects for the first time in radiative B meson decays!

Later, FCC-hh $p p$ collider could discover the Sparticles!

END

Thank you!

Backup Slides

2. MSSM with QFV

The basic parameters of the MSSM with QFV:

$$\{ \tan\beta, m_A, M_1, M_2, M_3, \mu, M^2_{Q,\alpha\beta}, M^2_{U,\alpha\beta}, M^2_{D,\alpha\beta}, T_{U\alpha\beta}, T_{D\alpha\beta} \}$$

(at $Q = 1 \text{ TeV}$ scale) ($\alpha, \beta = 1, 2, 3 = u, c, t$ or d, s, b)

$\tan\beta$: ratio of VEV of the two Higgs doublets $\langle H^0_2 \rangle / \langle H^0_1 \rangle$

m_A : CP odd Higgs boson mass (pole mass)

M_1, M_2, M_3 : $U(1), SU(2), SU(3)$ gaugino masses

μ : higgsino mass parameter

$M^2_{Q,\alpha\beta}$: left squark soft mass matrix

$M^2_{U\alpha\beta}$: right up-type squark soft mass matrix

$M^2_{D\alpha\beta}$: right down-type squark soft mass matrix

$T_{U\alpha\beta}$: trilinear coupling matrix of up-type squark and Higgs boson

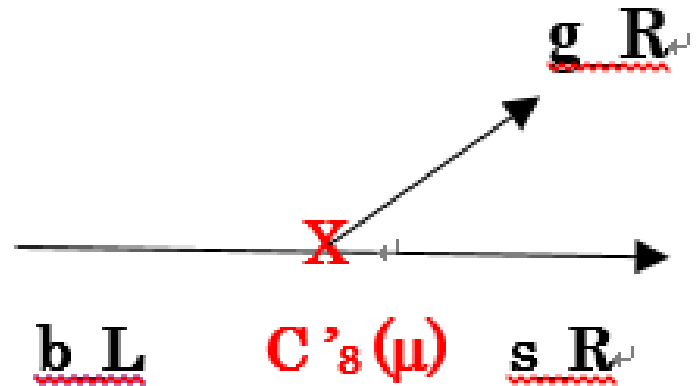
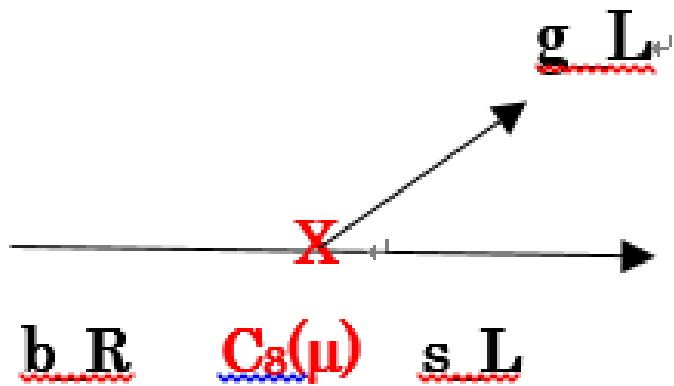
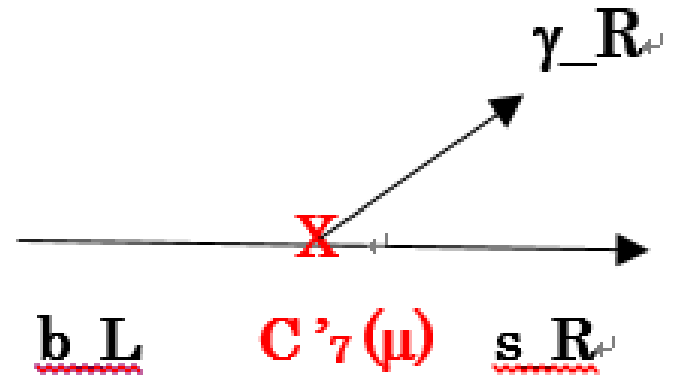
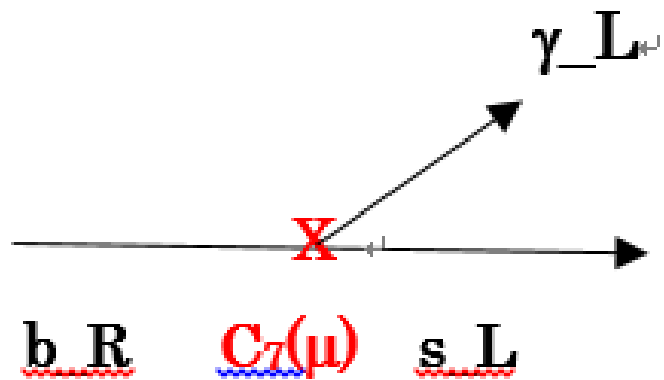
$T_{D\alpha\beta}$: trilinear coupling matrix of down-type squark and Higgs boson

We work in the MSSM with real parameters, except for the CKM matrix.

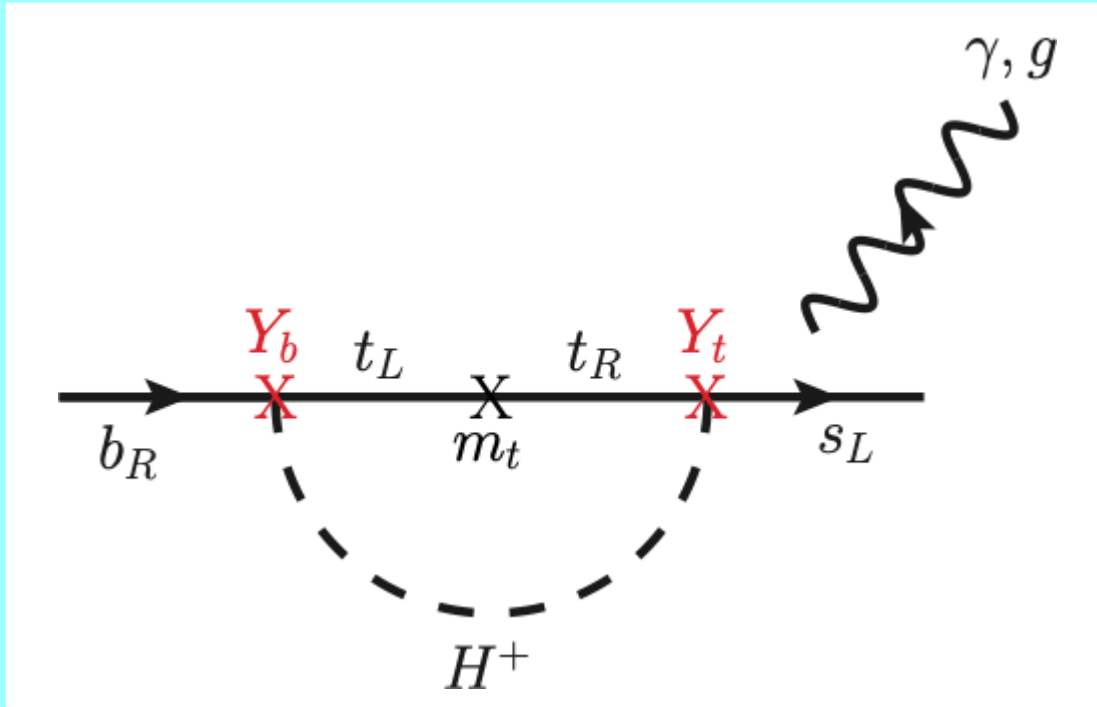
Constraints on the MSSM parameters from K & B meson and h^0 data:

Table 5: Constraints on the MSSM parameters from the K - and B -meson data relevant mainly for the mixing between the second and the third generations of squarks and from the data on the h^0 mass and couplings κ_b , κ_g , κ_γ . The fourth column shows constraints at 95% CL obtained by combining the experimental error quadratically with the theoretical uncertainty, except for $B(K_L^0 \rightarrow \pi^0 \nu \bar{\nu})$, m_{h^0} and $\kappa_{b,g,\gamma}$.

Observable	Exp. data	Theor. uncertainty	Constr. (95%CL)
$10^3 \times \epsilon_K $	2.228 ± 0.011 (68% CL) [21]	± 0.28 (68% CL) [40]	2.228 ± 0.549
$10^{15} \times \Delta M_K$ [GeV]	3.484 ± 0.006 (68% CL) [21]	± 1.2 (68% CL) [40]	3.484 ± 2.352
$10^9 \times B(K_L^0 \rightarrow \pi^0 \nu \bar{\nu})$	< 3.0 (90% CL) [21]	± 0.002 (68% CL) [21]	< 3.0 (90% CL)
$10^{10} \times B(K^+ \rightarrow \pi^+ \nu \bar{\nu})$	1.7 ± 1.1 (68% CL) [21]	± 0.04 (68% CL) [21]	$1.7_{-1.70}^{+2.16}$
ΔM_{B_s} [ps^{-1}]	17.757 ± 0.021 (68% CL) [21, 41]	± 2.7 (68% CL) [42]	17.757 ± 5.29
$10^4 \times B(b \rightarrow s \gamma)$	3.32 ± 0.15 (68% CL) [21, 41]	± 0.23 (68% CL) [11]	3.32 ± 0.54
$10^6 \times B(b \rightarrow s l^+ l^-)$ ($l = e$ or μ)	$1.60_{-0.45}^{+0.48}$ (68% CL) [43]	± 0.11 (68% CL) [44]	$1.60_{-0.91}^{+0.97}$
$10^9 \times B(B_s \rightarrow \mu^+ \mu^-)$	$2.69_{-0.35}^{+0.37}$ (68% CL) [45]	± 0.23 (68% CL) [46]	$2.69_{-0.82}^{+0.85}$
$10^4 \times B(B^+ \rightarrow \tau^+ \nu)$	1.06 ± 0.19 (68% CL) [41]	± 0.29 (68% CL) [47]	1.06 ± 0.69
m_{h^0} [GeV]	125.09 ± 0.24 (68% CL) [48]	± 3 [49]	125.09 ± 3.48
κ_b	$1.06_{-0.35}^{+0.37}$ (95% CL) [50]		$1.06_{-0.35}^{+0.37}$ (ATLAS)
	$1.17_{-0.61}^{+0.53}$ (95% CL) [51]		$1.17_{-0.61}^{+0.53}$ (CMS)
κ_g	$1.03_{-0.12}^{+0.14}$ (95% CL) [50]		$1.03_{-0.12}^{+0.14}$ (ATLAS)
	$1.18_{-0.27}^{+0.31}$ (95% CL) [51]		$1.18_{-0.27}^{+0.31}$ (CMS)
κ_γ	1.00 ± 0.12 (95% CL) [50]		1.00 ± 0.12 (ATLAS)
	$1.07_{-0.29}^{+0.27}$ (95% CL) [51]		$1.07_{-0.29}^{+0.27}$ (CMS)



$t - H^+$ loop contributions to $C_{7,8}(\mu_W)$:



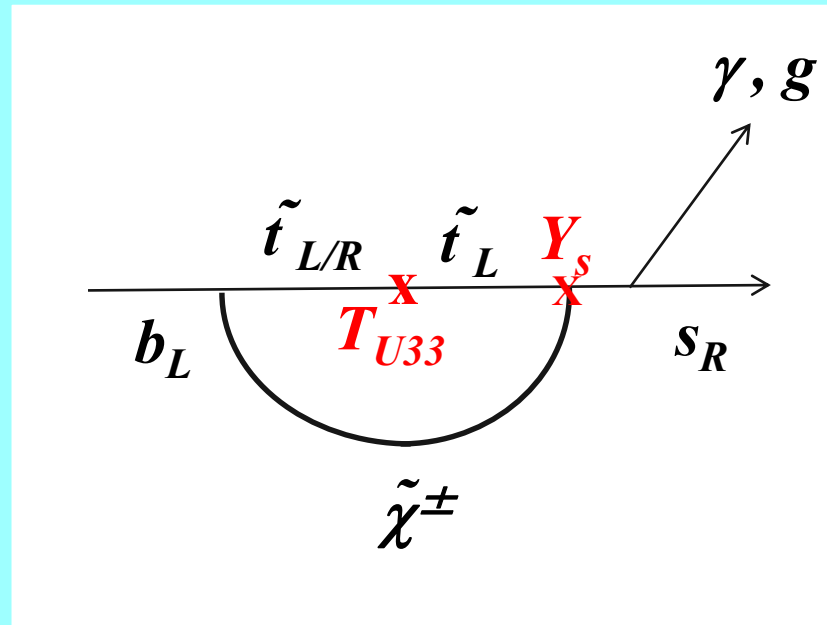
$Y_{b,t}$: bottom, top Yukawa coupling



$t - H^+$ loop contributions to $C_{7,8}(\mu_W)$ can be enhanced by large Y_b for large $\tan\beta$ and large Y_t !

$\tilde{t} - \tilde{t}$ loop contributions to $C'_{7,8}(\mu_W)$:

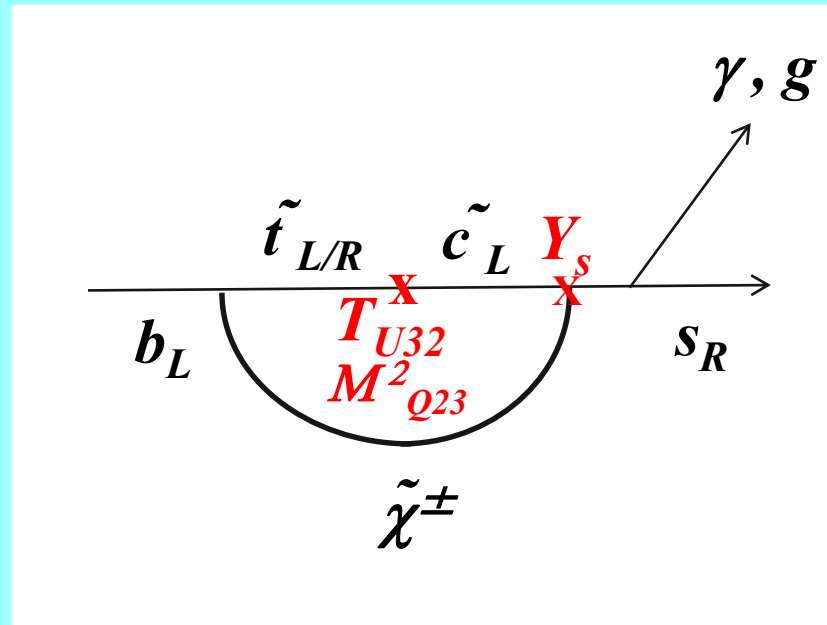
$$\tilde{\chi}^\pm \sim \tilde{W}^\pm + \tilde{H}^\pm$$



$\tilde{t} - \tilde{t}$ loop contributions to $C'_{7,8}(\mu_W)$ should be small due to very small Y_s !

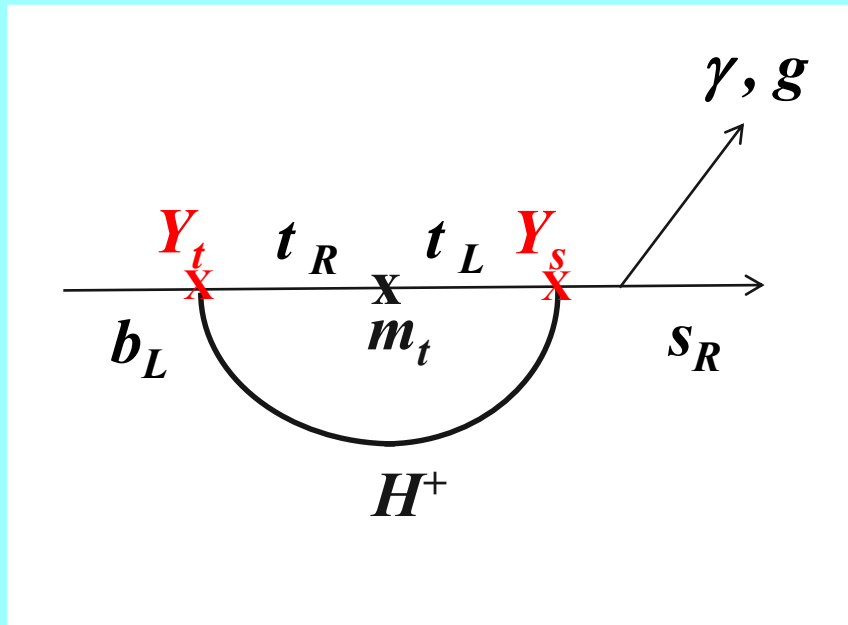
$\tilde{t} - \tilde{c}$ loop contributions to $C'_{7,8}(\mu_W)$:

$$\tilde{\chi}^\pm \sim \tilde{W}^\pm + \tilde{H}^\pm$$



$\tilde{t} - \tilde{c}$ loop contributions to $C'_{7,8}(\mu_W)$ should be small due to very small Y_s !

$t - H^+$ loop contributions to $C'_{7,8}(\mu_W)$:



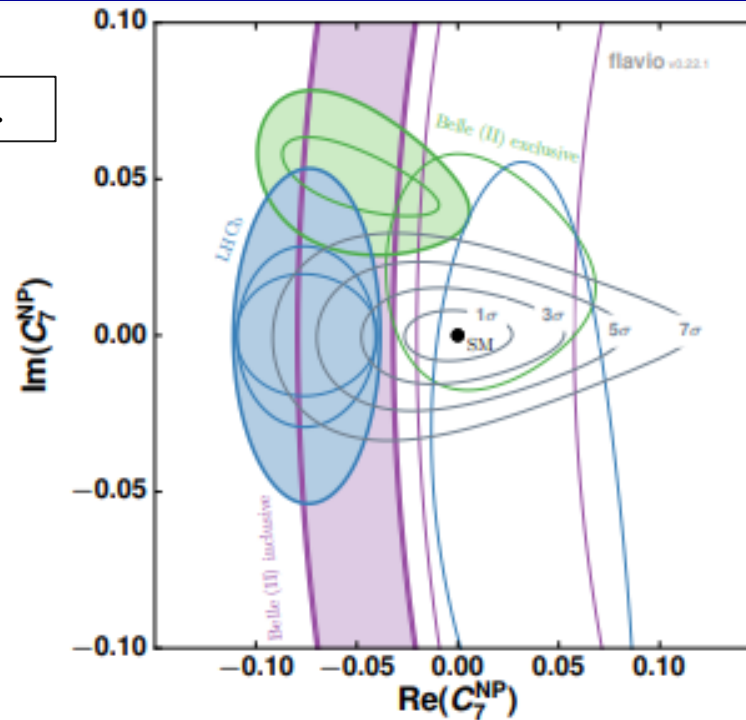
Y_t : top Yukawa coupling

Y_s : s quark Yukawa coupling



$t - H^+$ loop contributions to $C'_{7,8}(\mu_W)$ is small due to small Y_s .

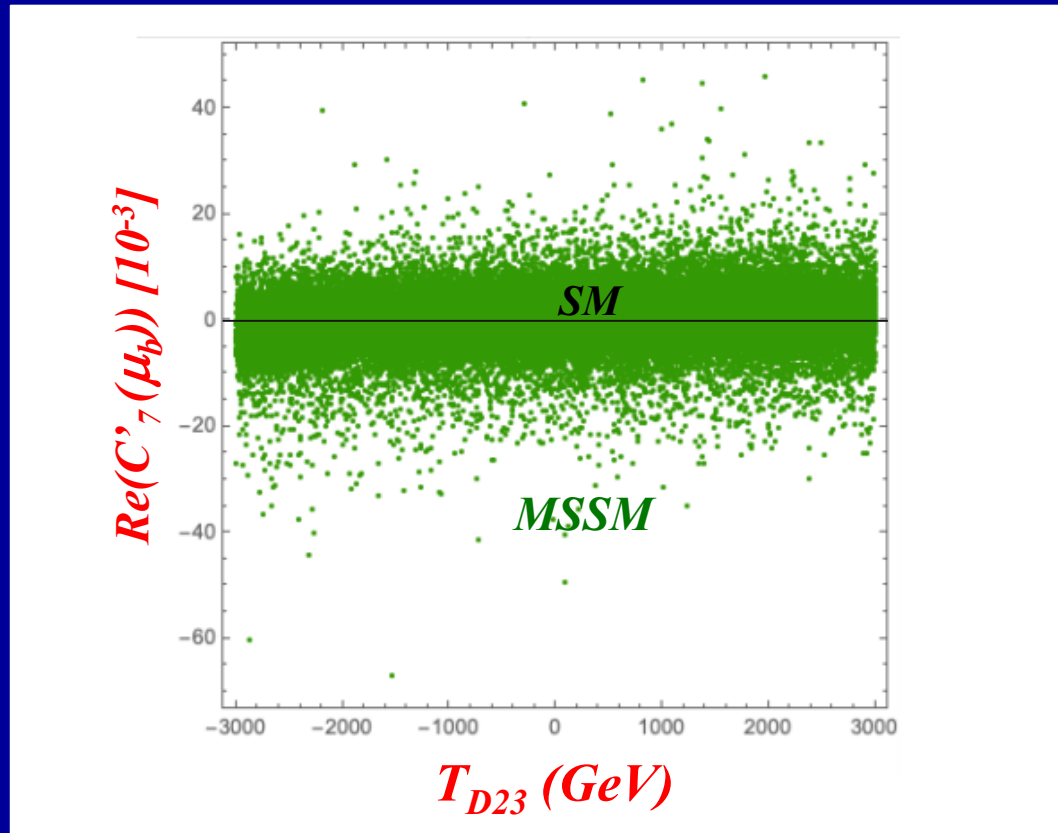
Albrecht et al., arXiv:1709.10308.



(c) $\text{Re}(C_7^{\text{NP}})$ versus $\text{Im}(C_7^{\text{NP}})$.

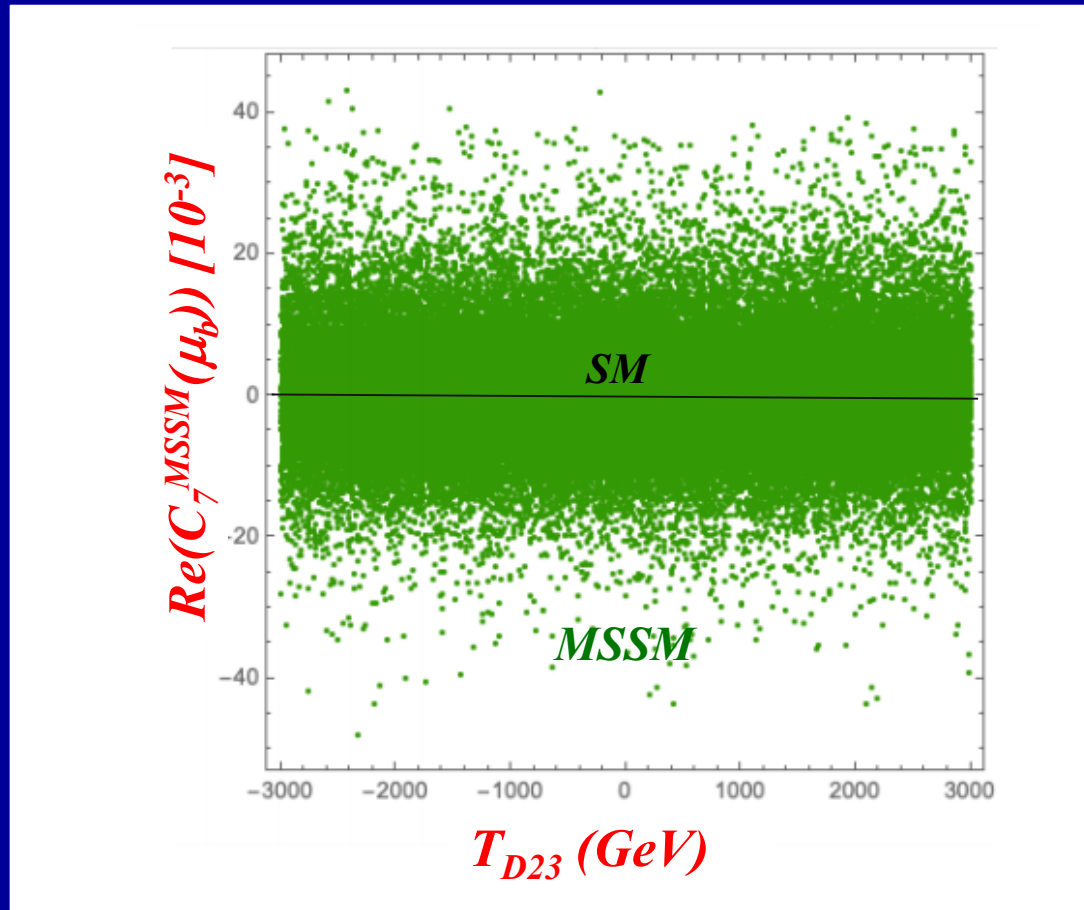
Figure 8: In the two-dimensional scans of pairs of Wilson coefficients, the current average (not filled) as well as the extrapolations to future sensitivities (filled) of LHCb at milestones I, II and III (exclusive) and Belle II at milestones I and II (inclusive and exclusive) are given. The central values of the extrapolations have been evaluated in the NP scenarios listed in Table 5. The contours correspond to 1σ uncertainty bands. The Standard Model point (black dot) with the 1σ , 3σ , 5σ and 7σ exclusion contours with a combined sensitivity of LHCb's 50 fb^{-1} and Belle II's 50 ab^{-1} datasets is indicated in light grey. The primed operators show no tensions with respect to the SM; hence no SM exclusions are provided.

Scatter plot in $T_{D23} - \text{Re}(C'_7(\mu_b))$ plane



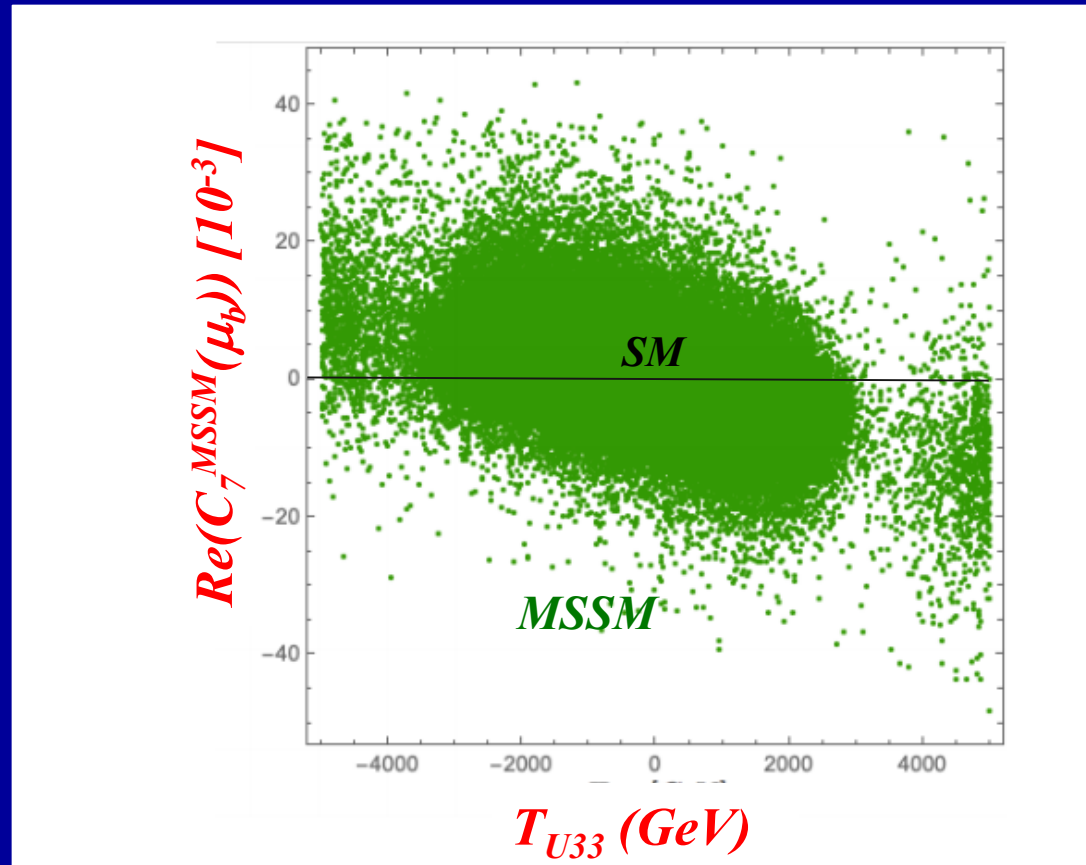
- *MSSM one-loop contributions to $\text{Re}(C'_7(\mu_b))$ can be large ($-0.07 \sim +0.05$) for large $|T_{D23}|$!*
- *There is an appreciable correlation between T_{D23} and $\text{Re}(C'_7(\mu_b))$!*

Scatter plot in $T_{D23} - \text{Re}(C_7^{\text{MSSM}}(\mu_b))$ plane



- MSSM one-loop contributions to $\text{Re}(C_7(\mu_b))$ can be large ($\sim \pm 0.05$) for any value of T_{D23} !

Scatter plot in $T_{U33} - \text{Re}(C_7^{MSSM}(\mu_b))$ plane



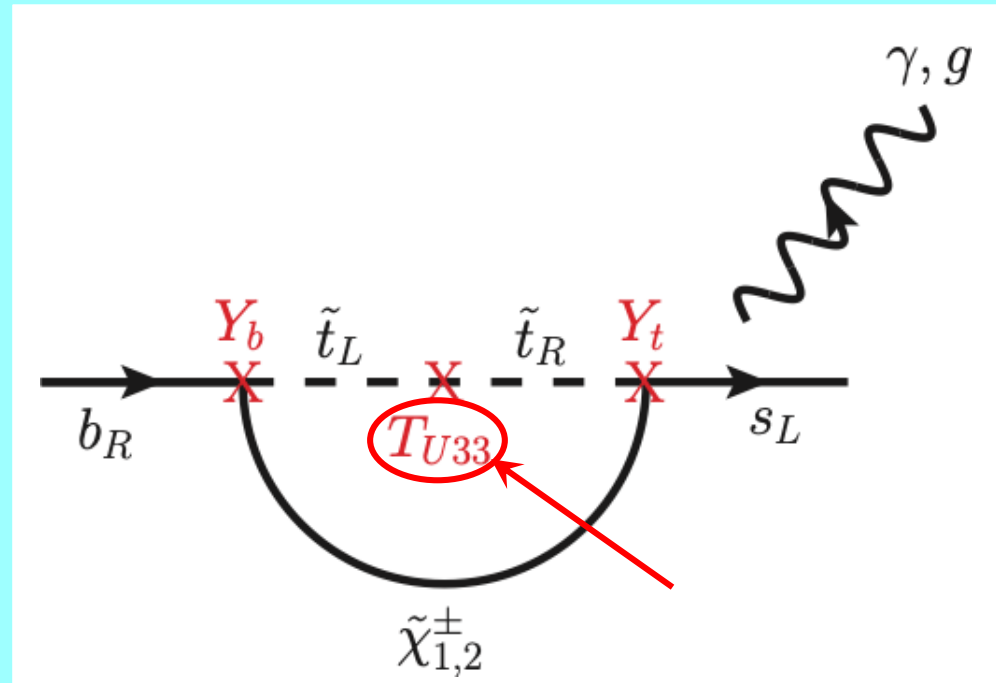
- *MSSM one-loop contributions to $\text{Re}(C_7(\mu_b))$ can be large ($\sim \pm 0.05$) for large T_{U33} !*
- *There is a significant correlation between T_{U33} and $\text{Re}(C_7^{MSSM}(\mu_b))$!*

$\tilde{t}_L - \tilde{t}_R$ loop contributions to $C_{7,8}(\mu_W)$:

$$\tilde{\chi}^\pm \sim \tilde{W}^\pm + \tilde{H}^\pm$$

Y_b : bottom Yukawa

Y_t : top Yukawa



$\tilde{t}_L - \tilde{t}_R$ loop contributions to $C_{7,8}(\mu_W)$ can be enhanced by large trilinear couplings T_{U33} and large Y_b for large $\tan\beta$ and large Y_t !

Physical masses for the benchmark scenario P1

Table 3: Physical masses in GeV of the particles for the scenario of Table 2.

$m_{\tilde{\chi}_1^0}$	$m_{\tilde{\chi}_2^0}$	$m_{\tilde{\chi}_3^0}$	$m_{\tilde{\chi}_4^0}$	$m_{\tilde{\chi}_1^+}$	$m_{\tilde{\chi}_2^+}$
800	812	925	2030	809	2030

m_{h^0}	m_{H^0}	m_{A^0}	m_{H^\pm}
124.9	4970	4970	4997

$m_{\tilde{g}}$	$m_{\tilde{u}_1}$	$m_{\tilde{u}_2}$	$m_{\tilde{u}_3}$	$m_{\tilde{u}_4}$	$m_{\tilde{u}_5}$	$m_{\tilde{u}_6}$
2934	1231	2986	3431	3656	4491	4493

$m_{\tilde{d}_1}$	$m_{\tilde{d}_2}$	$m_{\tilde{d}_3}$	$m_{\tilde{d}_4}$	$m_{\tilde{d}_5}$	$m_{\tilde{d}_6}$
836	3272	3416	3654	4489	4492

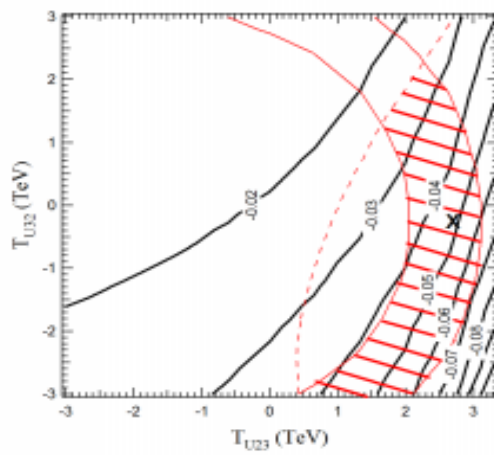
$m_{\tilde{\nu}_1}$	$m_{\tilde{\nu}_2}$	$m_{\tilde{\nu}_3}$	$m_{\tilde{l}_1}$	$m_{\tilde{l}_2}$	$m_{\tilde{l}_3}$	$m_{\tilde{l}_4}$	$m_{\tilde{l}_5}$	$m_{\tilde{l}_6}$
1506	1507	1582	1495	1496	1509	1509	1564	1652

Flavor decompositions of the squark mass eigenstates for the benchmark scenario P1

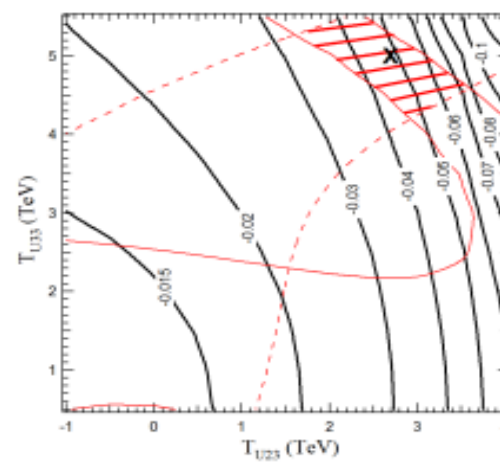
Table 4: Flavour decompositions of the mass eigenstates $\tilde{u}_{1,2,3}$ and $\tilde{d}_{1,2,3}$ for the scenario of Table 2. Shown are the expansion coefficients of the mass eigenstates in terms of the flavour eigenstates. Imaginary parts of the coefficients are negligibly small.

	\tilde{u}_L	\tilde{c}_L	\tilde{t}_L	\tilde{u}_R	\tilde{c}_R	\tilde{t}_R
\tilde{u}_1	0	0.0016	0.0992	0	-0.4090	-0.9071
\tilde{u}_2	-0.0012	-0.0070	-0.0225	0	0.9104	-0.4130
\tilde{u}_3	0.0660	0.2921	0.9491	0	0.0607	0.0770
	\tilde{d}_L	\tilde{s}_L	\tilde{b}_L	\tilde{d}_R	\tilde{s}_R	\tilde{b}_R
\tilde{d}_1	0	0	0.0059	0	0.4057	0.9140
\tilde{d}_2	0	0.0059	0.0289	0	-0.9137	0.4054
\tilde{d}_3	0	0.2898	0.9566	0	0.0245	-0.0172

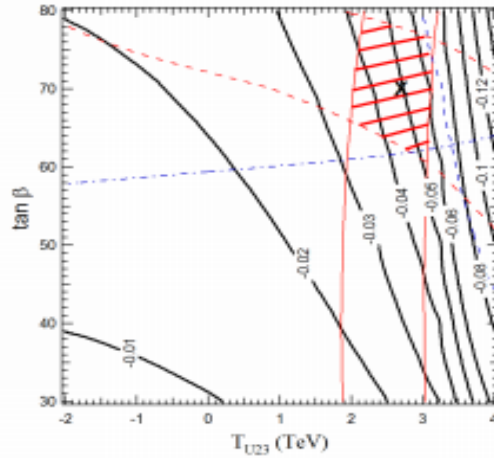
*Contour plots of the WCs
around the benchmark point P1*



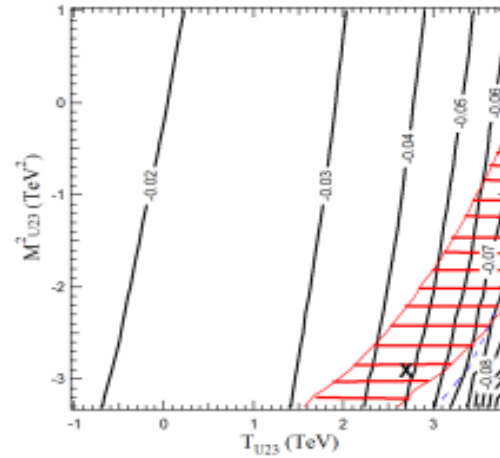
(a)



(b)



(c)



(d)

Figure 10: Contour plots of $Re(C'_7(\mu_b))$ around the benchmark point P1 in the parameter planes of (a) $T_{U23} - T_{U32}$, (b) $T_{U23} - T_{U33}$, (c) $T_{U23} - \tan\beta$, and (d) $T_{U23} - M_{U23}^2$. The parameters other than the shown ones in each plane are fixed as in Table 2. The "X" marks P1 in the plots. The red hatched region satisfies all the constraints in Appendix A. The red solid lines, the blue dashed lines, the red dashed lines and the blue dash-dotted lines show the m_{h^0} bound, the $B(b \rightarrow s\gamma)$ bound, the $B(B_s \rightarrow \mu^+\mu^-)$ bound, and the $m_{\tilde{d}_1}$ bound, respectively.

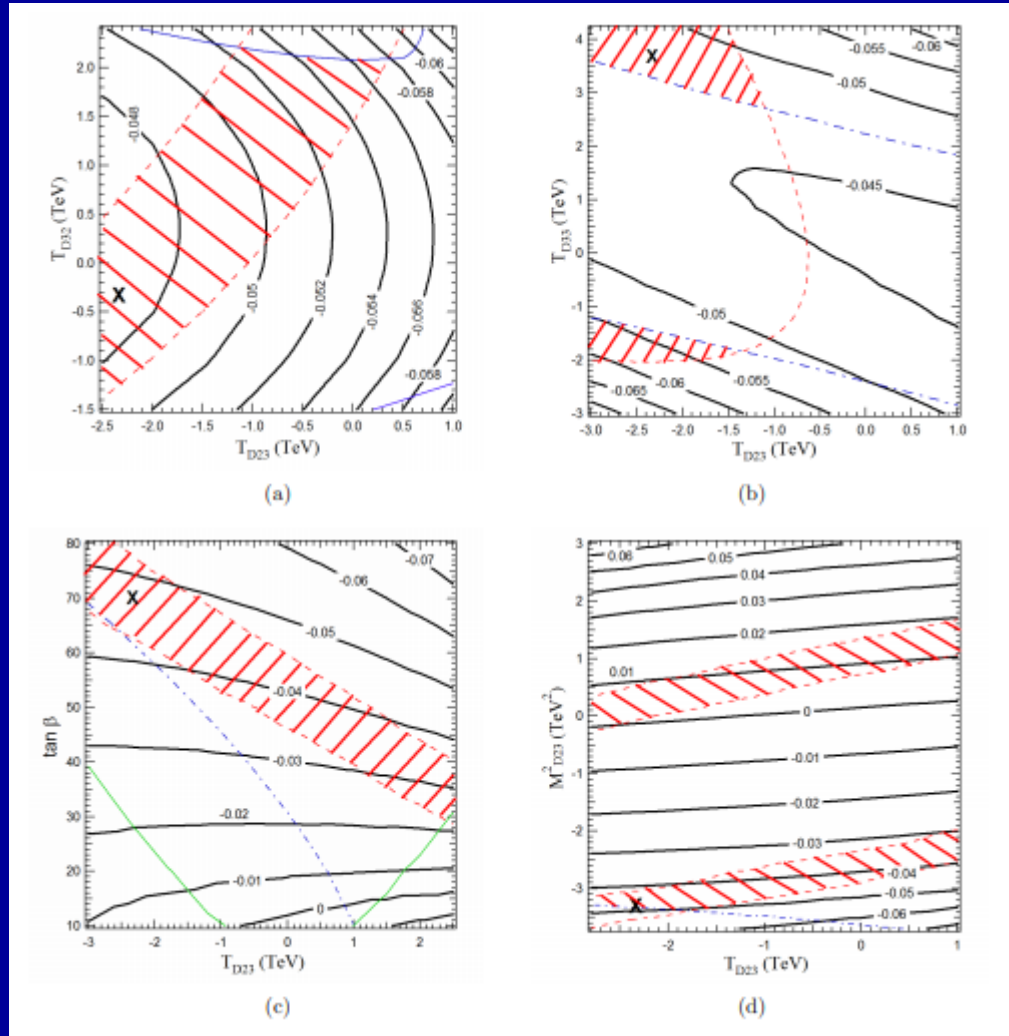


Figure 11: Contour plots of $Re(C'_7(\mu_b))$ around the benchmark point P1 in the parameter planes of (a) $T_{D23} - T_{D32}$, (b) $T_{D23} - T_{D33}$, (c) $T_{D23} - \tan \beta$, and (d) $T_{D23} - M_{D23}^2$. The parameters other than the shown ones in each plane are fixed as in Table 2. The "X" marks P1 in the plots. The red hatched region satisfies all the constraints in Appendix A. The definitions of the bound lines are the same as in Fig. 10. In addition to these the blue solid lines and the green solid lines show the ΔM_{B_s} bound and the vacuum stability bound on T_{D23} , respectively.

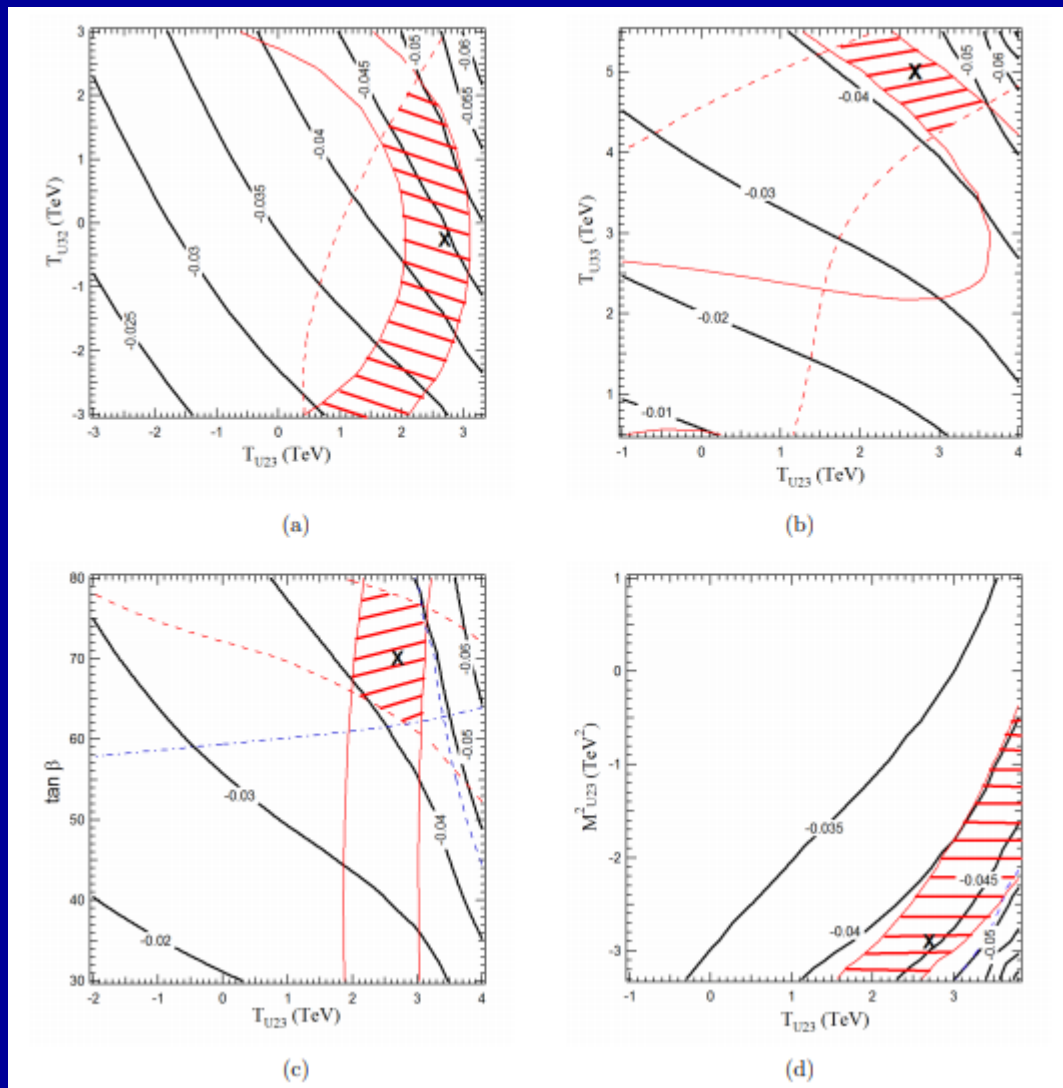


Figure 12: Contour plots of $Re(C_7^{MSSM}(\mu_b))$ around the benchmark point P1 in the parameter planes of (a) $T_{U23} - T_{U32}$, (b) $T_{U23} - T_{U33}$, (c) $T_{U23} - \tan \beta$, and (d) $T_{U23} - M_{U23}^2$. The parameters other than the shown ones in each plane are fixed as in Table 2. The "X" marks P1 in the plots. The red hatched region satisfies all the constraints in Appendix A. The definitions of the bound lines are the same as those in Fig. 10.

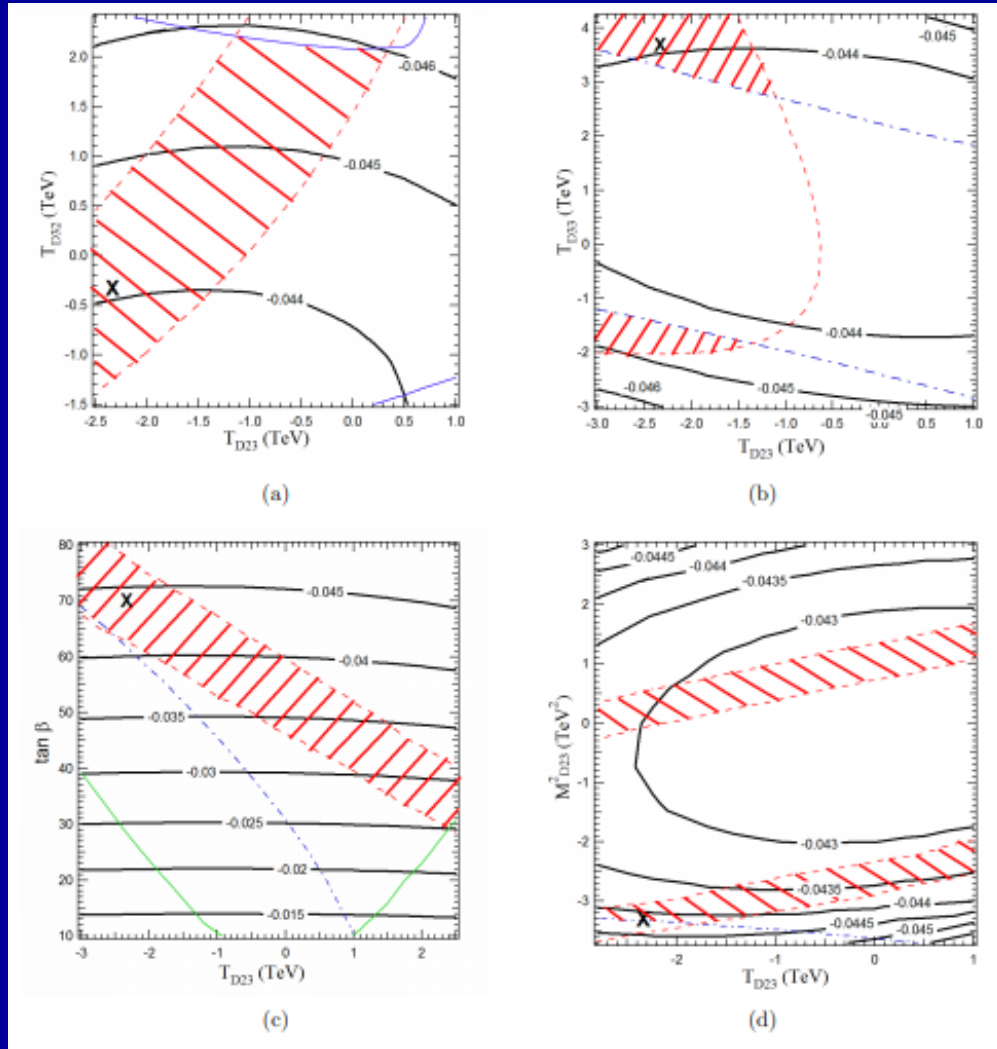


Figure 13: Contour plots of $Re(C_7^{MSSM}(\mu_b))$ around the benchmark point P1 in the parameter planes of (a) $T_{D23} - T_{D32}$, (b) $T_{D23} - T_{D33}$, (c) $T_{D23} - \tan\beta$, and (d) $T_{D23} - M_{D23}^2$. The parameters other than the shown ones in each plane are fixed as in Table 2. The "X" marks P1 in the plots. The red hatched region satisfies all the constraints in Appendix A. The definitions of the bound lines are the same as those in Fig. 11.